The Influence of Nodal Constriction on Conduction Velocity in Mylineated Nerve Fibers

J. A. Halter
J. W. Clark, Jr.

CRPC-TR93309
January 1993

Center for Research on Parallel Computation
Rice University
P.O. Box 1892
Houston, TX 77251-1892

neuroReport

NeuroReport 4, 89–92 (1993)

The influence of nodal constriction on conduction velocity in myelinated nerve fibers

J. A. Halter[1,CA] and J. W. Clark, Jr.[2]

[1]Division of Restorative Neurology and Human Neurobiology, Baylor College of Medicine, One Baylor Plaza, Houston, Texas 77030 and [2]Department of Electrical and Computer Engineering, Rice University, USA

[CA] Corresponding Author

MYELINATED nerve fibers exhibit a complex anatomy in the nodal region which includes a marked nodal-paranodal constriction and an intricate paranodal structure where the myelin sheath is separated from the axon by a narrow periaxonal space. In this study, a recently developed computational model of the mammalian myelinated nerve fiber based on electron microscopic data was employed to examine the effect of the nodal-paranodal axonal radius and periaxonal space width on the conduction of action potentials. These findings indicate that the nodal-paranodal constriction promotes higher conduction velocities by minimizing the component of the nodal capacity contributed by the paranodal axolemma. Model prediction of optimal nodal-paranodal radii is correlated with radii determined in experimental anatomical studies.

Key words: Anatomy; Computer simulation; Conduction velocity; Mathematics; Myelinated nerve fiber; Neurological models; Node of Ranvier

Introduction

The influence of the anatomical properties of the myelinated nerve fiber on the conduction of action potentials has been questioned since the early studies of Ranvier.[1] An important anatomical feature of the myelinated nerve fiber is the pronounced axonal constriction which can be present in the nodal region.[2,3] In their early work on saltatory conduction, Huxley and Stämpfli did not consider the effect of nodal constriction on conduction velocity to be significant due to the relatively short distance of the constriction.[4] This view has been largely held in the literature.

The discovery of the inhomogenous distribution and properties of ionic channels in the paranodal and internodal axon,[5–8] covered by the myelin sheath, has focused attention on their functional role. In order for these ionic channels to be active, ionic currents must be able to flow through these channels via the longitudinal pathway presented by the periaxonal space between the axon and the inner layer of the myelin sheath or transversely through the myelin sheath. The possibility for the presence of significant longitudinal currents in the paranodal periaxonal pathway has been described in a work using distributed-parameter models of amphibian and mammalian myelinated nerve fibers.[9] These models include a detailed representation of the nodal-paranodal anatomy derived from electron microscopic images of the ultrastructure of the node of Ranvier,[2,3] unlike previous theoretical studies relating fiber anatomy and conduction velocity.[10–16] In this report, we employ the distributed parameter model of the mammalian myelinated nerve fiber to examine the influence of the nodal-paranodal constriction on conduction velocity. Preliminary findings have been reported.[17,18]

Materials and Methods

Figure 1 presents a schematic of the nodal anatomy used to form the geometric parameters (Table 1) for the distributed-parameter model of a large-diameter (17 μm) mammalian myelinated nerve fiber. This model utilizes a non-uniform multi-segmented representation of this nodal anatomy as well as independent representation of the biophysical properties of the myelin sheath and underlying axolemma. Sodium (Na^+) and fast and slow-gated potassium (K^+) channels were included in the nodal, paranodal and internodal axolemmal membrane. Na^+ and K^+ channels were represented as specific permeabilities (cm s^{-1}). A temperature of 37°C was assumed. The details of the model are presented in a previous publication.[9] Ten nodes of Ranvier were represented, all with identical properties. The conduction velocity was computed using the time

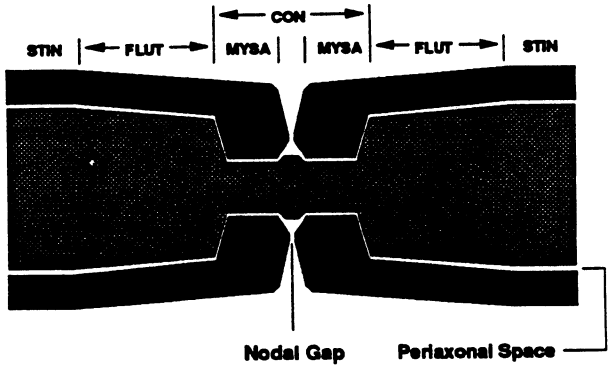

FIG. 1. Longitudinal-section detail of the nodal region for a large diameter myelinated nerve fiber. After the work of Berthold and Rydmark, CON represents the constricted region, MYSA the myelin sheath attachment region, FLUT the fluted region and STIN the stereotyped internodal region. This diagram is not to scale.

© Rapid Communications of Oxford Ltd

Table 1. Standard Geometric Parameters

NODE	
Length	1.5
Radius	2.5
Periaxonal space width (effective)	0.03
MYSA Section	
Length	4
Proximal radius	2.2
Distal radius	2.4
Periaxonal space width	0.001
Myelin sheath thickness	2.5
FLUT Section	
Length	75
Proximal radius (axial)	5.1
Distal radius (axial)	6.25
Proximal radius (radial)	9
Distal radius (radial)	6.25
Periaxonal space width	0.003
Myelin sheath thickness	2.5
STIN Section	
Length	1800
Radius	6.25
Periaxonal space width	0.004
Myelin sheath thickness	2.5

All dimensions are in units of μm. References to proximal and distal are relative to the node.

difference between the action potentials present at the two central nodes of Ranvier. The model was implemented on a Sequent Symmetry S81 parallel computer.

Results and Discussion

We first examined the influence of the width of the periaxonal space on conduction velocity. As the myelin sheath in the 4 μm long MYSA region was loosened (Fig. 2A), the conduction velocity slowed from an initial value of 66.5 m s^{-1} for a periaxonal space width of 0.01 nm, to 49.7 m s^{-1} at 10 nm, approaching a lower limit of 46.4 m s^{-1} for a width of 60 nm. As the periaxonal space width was increased uniformly along the entire length of the fiber (Fig. 2A), the conduction velocity decreased progressively, with conduction ceasing when the periaxonal space width reached 45.3 nm, as the axon effectively became demyelinated. Longitudinal current flow along the periaxonal space was virtually absent for small values of the periaxonal space width (Fig. 2B).

The axonal radius in the MYSA region was then varied while holding the width of the periaxonal space constant (Fig. 3A). In the case where the myelin sheath was effectively sealed to the axolemma (periaxonal space width of 0.01 nm), the conduction velocity reduced as the axon became progressively more constricted. For cases with a larger periaxonal space width, the conduction velocity increased initially and then decreased as the axon radius approached zero. Using the standard periaxonal space width in the MYSA region of 1 nm, the conduction velocity increased from 47.9 m s^{-1} to a maximum of 58.3 m s^{-1} as the axonal

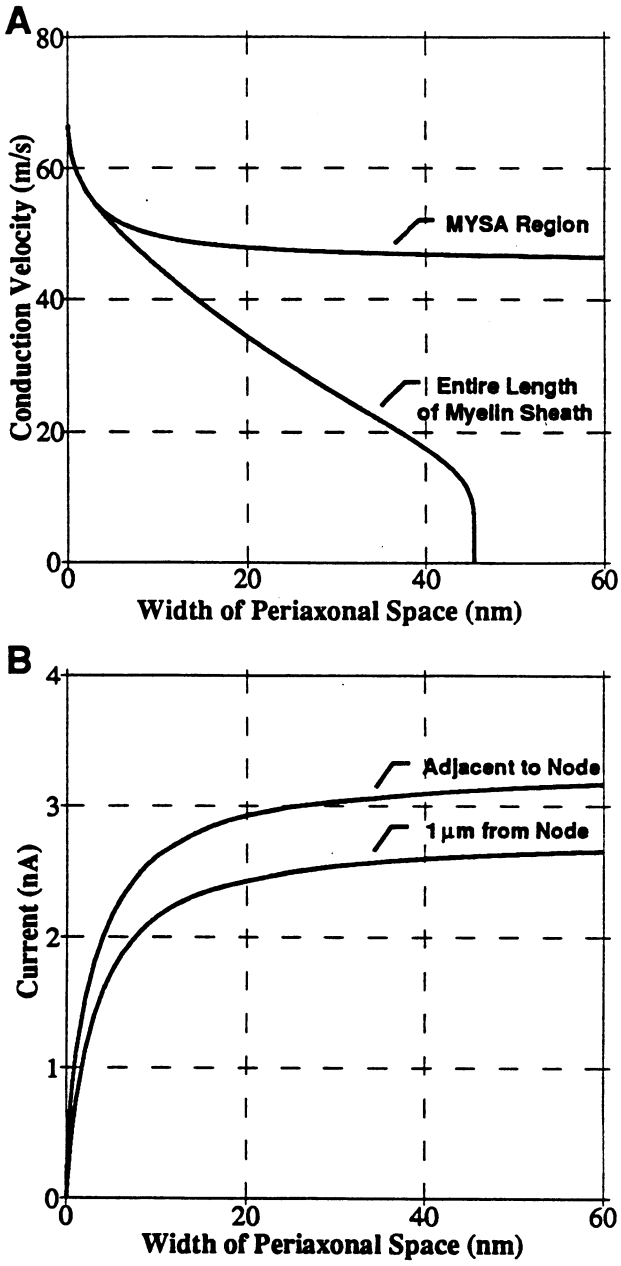

FIG. 2. (A) Conduction velocity versus the width of the periaxonal space. The upper curve shows the effect of increasing the periaxonal space width in the MYSA region alone. The conduction velocity slows as the node is loaded by the adjacent exposed axolemmal membrane and approaches a constant velocity. In the second case, the periaxonal space width under the length of the myelin sheath is uniformly increased. As the axon becomes effectively demyelinated, conduction stops. (B) Periaxonal longitudinal current versus the width of the periaxonal space in the MYSA region. The peak amplitudes of the periaxonal longitudinal currents immediately adjacent to the node and 1 μm from the node are shown.

radius was reduced to 22% (1.4 μm) of that present in the internode (6.25 μm). This represents an increase in conduction velocity of 22% for a periaxonal space width of 1 nm and an increase of 41% (51.1 m s^{-1} *vs* 36.3 m s^{-1}) for a periaxonal space width of 10 nm.

Simulation studies were then undertaken to determine the effect of simultaneous nodal and MYSA axo-

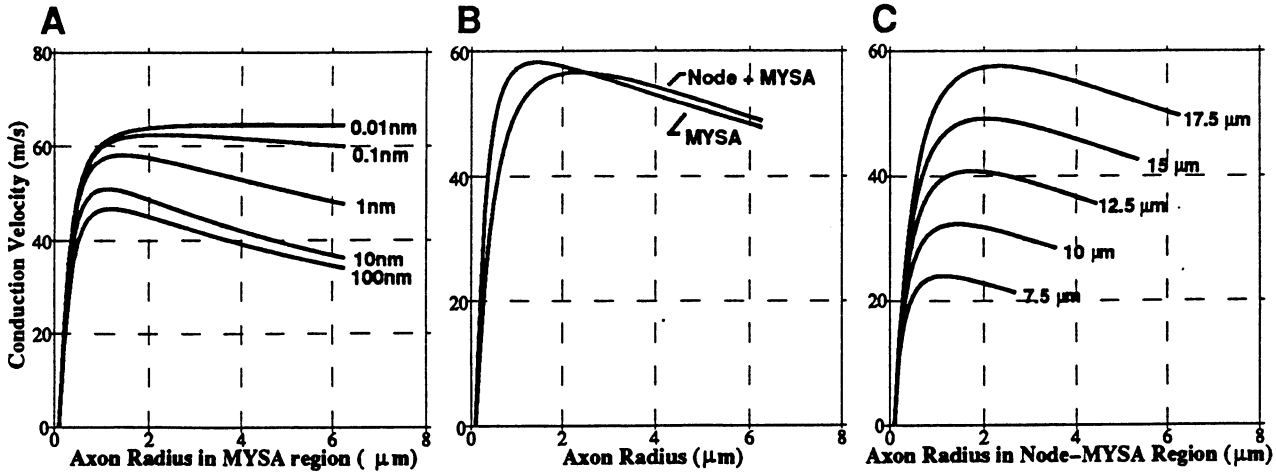

FIG. 3. (A) Conduction velocity versus the radius of the axon in the MYSA region. The various curves represent the relationship seen for different periaxonal space widths. (B) Comparison of the influence of the axon radius in the MYSA region alone versus the nodal and MYSA region on conduction velocity. Note the increase in conduction velocity for MYSA region axonal radii less than that present at the node. (C) Conduction velocity versus the radius of the axon at the node and MYSA region for fibers of various diameters.

nal constriction. When the radius of the axon at the node and in the MYSA region were both reduced, in comparison to the MYSA region alone (Fig. 3B), an axonal radius in the MYSA region which was 56% of the nodal radius resulted in an additional increase in the conduction velocity of 3%. These findings indicate a functional advantage to an increased axonal constriction in the MYSA region as noted in the anatomical studies of Berthold and Rydmark.[2]

Examination of the influence of constriction of the nodal and MYSA region axonal radius for a range of fiber diameters resulted in an increase in conduction velocity for all cases studied (Fig. 3C). The following expression was used to relate the internodal radius (R_{IN}) to the nodal radius (R_N),

$$R_{IN} = C_0 + C_1 R_N$$

Using the axonal radii at which the peak conduction velocities were reached, a least-squares fit to this expression was performed using Mathematica.[19] The coefficients $C_0 = -0.24$ and $C_1 = 3.3$ were found to provide a minimal error. These values correlate well with the experimental findings of Rydmark[20] who studied the internodal and nodal axonal radii of single myelinated nerve fibers in young adult cats and found a mean value for C_0 of −0.67 with a range of −1.42 to +0.19 and a mean value for C_1 of 2.72 with a range of 2.13–3.32.

We anticipated the reduction in the conduction velocity produced as the width of the periaxonal space in the MYSA region was increased. It is reasonable to expect that the additional capacitive load presented to the node of Ranvier by the exposed paranodal axon coupled to the node through an increased periaxonal space should slow conduction. This finding correlates to that of Hines and Shrager[21] who reported significant conduction delays in their simulations when the space between the myelin sheath and the axon was increased over a length of 100 μm in the paranodes.

The increase in periaxonal longitudinal current flow as the periaxonal space width grows reflects the increased coupling of the paranodal axon to the node. For longitudinal periaxonal currents to exist, there must be charge displacement along the periaxonal space. If the periaxonal longitudinal current is primarily due to the flow of ions, the conduction velocity would be expectd to be higher than that shown in Figures 2 and 3 for periaxonal space widths of the same order as the diameter of the ions. The effective hydrated diameter is estimated to be 0.33 nm for potassium ions and 0.27 nm for sodium ions.[22] However, the cross-sectional shape of the actual periaxonal space in the MYSA region is not a simple annulus as is assumed in the model. Electron microscopic studies[23,24] indicate that there are particles about 10 nm in diameter bridging the periaxonal space, with a center-to-center spacing of 12.5–15 nm. This results in a space of 2.5–5 nm between these particles, a blockage of two-thirds of the available space. The width of the periaxonal space was found to be 2–3 nm,[23] providing ample space for the passage of either sodium or potassium ions. Using an axonal radius of 4.6 μm, the effective equivalent periaxonal space width is 1 nm, as utilized in our model.[9] An additional electron microscopic study[25] reports similar dimensions, with particles 16 nm in width spaced 20 nm center-to-center. This results in a space between particles of 4 nm, a blockage of four-fifths of the available space. Assuming that there is not a dramatic reduction in the space between these particles, there should be sufficient space to allow for passage of either potassium or sodium ions.

We did not anticipate an increase in conduction velocity as the axon in the MYSA region was constricted. With a reduction in axon radius in the MYSA region,

the reduction in capacitance dominates over the progressively increasing intra-axonal longitudinal resistance until the MYSA radius is on the order of one sixth of the internodal radius. Thus, our simulation studies predict that the presence of a nodal constriction appears to be a mechanism for the optimization of conduction velocity. Indeed, the relative dimensions of the nodal and MYSA region axonal radii that maximize conduction velocity in this model correlate well with the radii determined by electron microscopic observation[2,3]

Our results are at variance with those of Moore *et al.*[14] They simulated nodal constriction by reducing the nodal area to one-half the normal value within a uniform Δz step on the order of 200 μm in length, calculating a reduction in conduction velocity of only 3.8%. This points out a fundamental distinction between the models employed. The non-uniform Δz step technique utilized in our model[9] allows for a more accurate representation of the nodal and MYSA region geometry. Most importantly, the representation of the periaxonal space is necessary for proper simulation of the functional implications of the ultrastructure of the node of Ranvier as well as the ionic channels present in the paranodal axolemma.

Conclusion

Our results indicate that the conduction velocity in myelinated nerve fibers is sensitive to minor changes in the paranodal periaxonal space width. The sensitivity to this parameter may be one that is either exploited by the fiber for minor adjustments in performance or one that could have a significant influence on the conduction properties of nerve fibers suffering from trauma or other pathology which would disrupt the myelin sheath in the attachment region. The constriction in the nodal region provides both a reduction in the nodal capacity by minimizing the nodal area as well as reducing the contribution of the paranodal axolemmal membrane by restricting conductance along the periaxonal pathway. The degree of nodal constriction at which a near maximal conduction velocity is obtained in our modeling study is very close to that found in experimental studies. This points to yet another functional advantage of the biophysical properties of the myelinated nerve fiber; a neural structure that has been thought of as simple, but continues to reveal more complexity on further examination.

References

1. Ranvier LA. *Comptes Rendus des Seances de l'Academic des Sciences* **73**, 1168–1171 (1871).
2. Berthold C-H and Rydmark M. *Experientia* **39**, 964–976 (1983).
3. Berthold C-H and Rydmark M. *J Neurocytol* **12**, 475–505 (1983).
4. Huxley AF and Stämpfli R. *J Physiol (London)* **108**, 315–339 (1949).
5. Bostock H and Sears T. *J Physiol (London)* **280**, 273–301 (1978).
6. Brismar T. *Acta Physiol Scand* **113**, 167–176 (1981).
7. Chiu SY and Ritchie JM. *J Physiol (London)* **313**, 415–437 (1981).
8. Shrager P. *J Physiol (London)* **392**, 587–602 (1987).
9. Halter JA and Clark Jr, JW. *J Theo Biol* **148**, 345–382 (1991).
10. Brill MH, Waxman SG, Moore JW *et al. J Neurol Neurosurg Psych* **40**, 769–774 (1977).
11. Dun FT. *IEEE Trans Biomed Eng* **17**, 21–24 (1970).
12. Fitzhugh R. *Biophys J* **2**, 11–21 (1962).
13. Goldman L and Albus JS. *Biophys J* **8**, 596–607 (1968).
14. Moore JW, Joyner RW, Brill MH *et al. Biophys J* **21**, 147–160 (1978).
15. Rushton WAH. *J Physiol (London)* **115**, 101–122 (1951).
16. Smith RS and Koles ZJ. *Am J Physiol* **219**, 1256–1258 (1970).
17. Halter JA and Clark Jr, JW. *Soc Neurosc Abstr* **15**, 376 (1989).
18. Halter JA, Clark Jr, JW. *Proc Ann Int Conf IEEE Eng Med Biol Soc* **11**, 1261–1262 (1989).
19. Wolfram S. *Mathematica, A System for Doing Mathematics by Computer.* Redwood City: Addison-Wesley Publishing Company, 1991.
20. Rydmark M. *Neurosc Lett* **24**, 247–250 (1981).
21. Hines M and Shrager P. *Restor Neurol Neurosc* **3**, 81–93 (1991).
22. Klotz IM. Water: Its fitness as a molecular environment. In: *Membranes and Ion Transport.* London: Wiley-Interscience, 1970: 93–122.
23. Livingston RB, Pfenninger K, Moor H *et al. Brain Res* **58**, 1–24 (1973).
24. Schnapp B, Peracchia C and Mugnaini E. *Neurosci* **1**, 181–190 (1976).
25. Wiley CA and Ellisman MH. *J Cell Biol* **84**, 261–280 (1980).

ACKNOWLEDGEMENTS: Use of the Sequent Symmetry S81 computer was provided by the Center for Research on Parallel Computation, Rice University, under NSF Cooperative Agreement No. CCR-9120008. Support for this effort was generously provided by the Vivian L. Smith Foundation for Restorative Neurology and the Whitaker Foundation.

Received 16 October 1992; accepted 20 November 1992